# Design optimization for improved HQ and performance of a DEP aircraft

David Planas, Carsten Döll, Philippe Pastor, Eric Nguyen Van

# Design optimization for improved performance of a DEP aircraft

David Planas*
*ISAE-Supaero, DCAS, Toulouse, France, 31400*
*ONERA, DTIS, Toulouse, France, 31400*

Carsten Döll†
*ONERA, DTIS, Toulouse, France, 31400*

Philippe Pastor‡
*ISAE-Supaero, DCAS, Toulouse, France, 31400*

Eric Nguyen Van§
*ONERA, DTIS, Toulouse, France, 31400*

**Through an adequate preliminary design and analysis, the aero-propulsive synergistic effects present in DEP aircraft can be exploited to increase the overall capacities and system efficiency. This paper is divided into two main sections. The first one examines the impact of aero-propulsive coupling on aircraft architecture when modified during the preliminary design. Specifically, the propeller's potential to increase lift is investigated. A built-in aerodynamic module is proposed as an approach for this purpose, using the all-electric NASA X-57 experimental concept as the reference aircraft. The second section focuses on several single-point constrained multidisciplinary optimizations aimed at maximizing lift generated through the interaction, reducing the stall speed, and minimizing the required installed power. The developed aerodynamic database is implemented into a nonlinear flight dynamics model, enabling the aircraft to be trimmed at the resultant stall speed. The resultant optimized configurations are able to reduce the stall speed up to 3.2 %, or the power utilized by the HLPs up to 8.27 %, while maintaining the same wing loading and stall speed.**

**Keywords: DEP, aero-propulsive interaction, augmented lift, handling qualities**

## Nomenclature

**Symbols**

| | | |
|---|---|---|
| $m$ | = | Mass of the aircraft (kg) |
| $g$ | = | Gravitational acceleration (m.s$^{-2}$) |
| $\rho$ | = | Air density (kg.m$^{-3}$) |
| $S_w$ | = | Wing surface (m$^2$) |
| $c$ | = | Mean aerodynamic chord (m) |
| $b$ | = | Wingspan (m) |
| $V$ | = | Airspeed (m.s$^{-1}$) |
| $V_{SR}$ | = | Stall speed (m.s$^{-1}$) |
| $T$ | = | Thrust (N) |
| $P$ | = | Power (W) |
| $\alpha$ | = | Angle of attack (°) |
| $\beta$ | = | Side-slip angle (°) |
| $\gamma$ | = | Flight path angle (°) |

*Ph.D., david.planas-andres@isae-supaero.fr
†Research engineer, carsten.doll@onera.fr
‡Professor Researcher, philippe.pastor@isae.fr
§Researcher engineer, eric.nguyen_van@onera.fr

| | | |
|---|---|---|
| $\theta$ | = | Pitch angle (°) |
| $\phi$ | = | Roll angle (°) |
| $\boldsymbol{\omega}$ | = | Angular velocity in body frame (rad.s$^{-1}$) |
| $\delta_a$ | = | Ailerons deflection (°) |
| $\delta_e$ | = | Elevator deflection (°) |
| $\delta_R$ | = | Rudder deflection (°) |
| $\delta_f$ | = | Flap position (°) |
| $\delta_x$ | = | Thrust setting of the HLPs (-) |
| $C_L, C_D, C_Y$ | = | Lift, drag and lateral force coefficients (-) |
| $C_l, C_m, C_n$ | = | Roll, pitch and yaw moment coefficients (-) |
| $C_T, C_{mT}$ | = | Thrust force pitch-moment coefficients (-) |
| $n$ | = | Propeller angular speed (rad.s$^{-1}$) |
| $x_p$ | = | Propeller offset to the wing's leading edge (m) |
| $i_p$ | = | Propeller installation angle (°) |
| $D_p$ | = | HLPs diameter (m) |
| $f_p$ | = | HLPs power fraction (-) |
| $\boldsymbol{x_i}$ | = | Position of HLP $i^{th}$ in body frame (m) |
| $N_p$ | = | Number of propellers |
| $M$ | = | Number of Mach (-) |

**Sub- and Superscripts**

| | | |
|---|---|---|
| $SR$ | = | Stall |
| $w$ | = | Wing |
| $p$ | = | HLP propeller |
| $b$ | = | Body frame |
| $T$ | = | Thrust |
| $*$ | = | Optimum |
| $max$ | = | Maximum |
| 0 | = | Conventional configuration |

**Acronyms**

| | | |
|---|---|---|
| DEP | = | Distributed Electric Propulsion |
| HLP | = | High Lift Propeller |
| MDO | = | Multidisciplinary Optimization |

# I. Introduction

Distributed Electric Propulsion (DEP) is an emerging and disruptive technology with promising potential to meet the increasingly demanding environmental requirements. Aside from the environmental aspect, the most promising feature relies on the capacity to leverage the new interactions that emerged between the propulsive group and the lifting surfaces [1].

One of the most interesting ways to leverage the interaction is to enhance the overall lift. Wings of General Aviation (GA) aircraft are usually compromised in design, as the wing surface is larger than optimal for cruise to meet the imposed stall speed $V_{SR}$. Thanks to the augmented dynamic pressure in the slipstream behind the propeller, higher wing loadings are reachable [2]. The maximum lift coefficient $C_{L_{MAX}}$ to meet the required $V_{SR}$ can then be achieved without over-dimensioning the wing. Propellers with such an aim have been called High Lift Propellers (HLPs), and have been demonstrated in several aircraft concepts like NASA X-57 Maxwell [3], or ONERA AMPERE's concept [4]. In AMPERE e.g., this augmentation of lift is sufficient to dispense with flaps, eliminating a mechanism. Even without leveraging these interactions, DEP concepts offer potential benefits. Nguyen Van et al. proved the feasibility of providing lateral control through differential thrust thanks to the faster response of electrical engines [5],[6],[7]. This allows the reduction of the vertical tail and the associated friction drag and mass.

Since DEP propellers are given additional purposes apart from the pure propulsion of the airplane, it is clear that the architecture of such an aircraft will differ from that of a conventional one. The number of propellers, their geometry, and their installation setup can substantially change the aero-propulsive coupling. It is reasonable to expect that depending on the desired application, there will exist an optimal design. Moreover, it is a common practice to uniform propeller installation geometry during the design to ease the construction, e.g. in the X-57 [8]. However, when operating with HLPs, an optimal design would involve different installation geometries for each propeller since local flow conditions vary across the wingspan [9]. This paper is focused on the enhancing-lift feature of the propellers. The objective is to optimize the installation parameters that lead to maximum leverage of the interaction for lift-enhancing purposes in order to meet the required stall speed $V_{SR}$.

Several authors have investigated the effects of the propeller installation on the interaction. Gentry et al. [10] and Veldhuis [11] studied the influence of the main variables of interest within the installation of propellers. A recent study by Fei et al. [9] explores extensively the geometry effects for a large number of variables focusing on lift augmentation. All these studies offer a good insight into the behavior of the interaction to optimize the architecture. The optimization is, however, an arduous problem. Analytical or traditional empirical methods are unable to capture the effects of the interactions. Several studies have performed optimization under propeller-wing interaction [12], [13], [14], generally focusing on the wing. In order to capture properly the effects of drag, higher fidelity methods are required, which in turn, reduces the flexibility when varying the main propeller-related installation and geometry variables, generally prefixing their number. Indeed, if these parameters are to be quickly mapped within the iterative design, a compromise to model the effects of the aero-propulsive couple is needed. This has motivated the use of surrogate models extracted from wind-tunnel or CFD analyses [15], [8], or of simpler analytic models in conjunction with Vortex Lattice Method (VLM) tools [16]. Although higher fidelity methods can be avoided if drag is not involved in the optimization, a sufficient amount of fidelity in its computation is required if the aircraft is to be trimmed.

In order to study the interaction's effects, a modified VLM approach is taken. A pre-generated aerodynamic database produced with OpenVSP [17]. The aerodynamic coefficients are treated and modified through a coupling method to account for the aero-propulsive interaction. The aerodynamic module is coupled with a non-linear six-degrees-of-freedom (DOF) flight dynamics model in order to trim the aircraft. The whole module is built in Python. This paper is organized as follows. In section II, the aerodynamic and 6 DOF module is briefly introduced and validated using available analyses. In section III a sensitivity analysis is performed. Several propeller-architecture configurations are tested and the effects on the lift are presented and analyzed. In section IV, the stall speed of the original X-57 is calculated through constrained minimization. Finally, in section V, several single-point multidisciplinary optimizations are carried out with the aim of reducing the stall speed, increasing the lift, and minimizing the installed power. Results are discussed in section VI.

## II. Problem-modeling and aerodynamic database

The following section explains the mathematical formulation and the means to model the problem and calculate the aerodynamic forces and moments in the presence of the aero-propulsive coupling. First, the flight equations are recalled, then it is explained how the aerodynamic database is obtained. After, a reference aircraft is chosen, and the thrust modeling is presented, and finally, the model is validated with high-fidelity numeric methods.

### A. Equations of flight

Euler's equations of motion are used. Equations are projected in the body frame and uniform wind velocity is assumed. Equations in this form can be directly found in [18]:

$$\begin{pmatrix} m(\dot{u} - rv + qw) \\ m(\dot{v} + ru - pw) \\ m(\dot{w} - qu + pv) \end{pmatrix} = mg \begin{pmatrix} -\sin\theta \\ \cos\theta\sin\phi \\ \cos\theta\cos\phi \end{pmatrix} + \begin{pmatrix} F_{T,xb} \\ F_{T,yb} \\ F_{T,zb} \end{pmatrix} + \frac{1}{2}\rho S_w V^2 \mathbf{H_{ba}} \begin{pmatrix} -C_D \\ C_Y \\ -C_L \end{pmatrix} \tag{1}$$

$$\mathbf{I}\begin{pmatrix} \dot{p} \\ \dot{q} \\ \dot{r} \end{pmatrix} + \begin{pmatrix} p \\ q \\ r \end{pmatrix} \times \mathbf{I}\begin{pmatrix} p \\ q \\ r \end{pmatrix} = \frac{1}{2}\rho S_w V^2 l \begin{pmatrix} C_l \\ C_m \\ C_n \end{pmatrix} + \begin{pmatrix} M_{T,xb} \\ M_{T,yb} \\ M_{T,zb} \end{pmatrix} \tag{2}$$

Being $\mathbf{I}$ the inertia matrix, and $\mathbf{H_{ba}}$ the rotation matrix from aerodynamic frame to body reference in order to add the aerodynamic forces $\frac{1}{2}\rho S V^2 (C_D, C_Y, C_L)^T$. The length $l$ represents the aerodynamic chord $c$ for the longitudinal coefficients, and the wingspan $b$ for the lateral ones.

$$\mathbf{H_{ba}} = \begin{pmatrix} \cos\alpha\cos\beta & -\cos\alpha\sin\beta & -\sin\alpha \\ \sin\beta & \cos\beta & 0 \\ \sin\alpha\cos\beta & -\sin\alpha\sin\beta & \cos\alpha \end{pmatrix} \tag{3}$$

The angle of attack $\alpha$ and the side-slip angle $\beta$, together with the aerodynamic airspeed $V$ can be used for convenience:

$$V = \sqrt{u^2 + v^2 + w^2}, \qquad \beta = \arcsin\frac{v}{V}, \qquad \alpha = \arctan\frac{w}{u} \tag{4}$$

The so-called inverse angular kinematic equations are:

$$\begin{pmatrix} \dot{\phi} \\ \dot{\theta} \\ \dot{\psi} \end{pmatrix} = \begin{pmatrix} 1 & \sin\phi\tan\theta & \cos\phi\tan\theta \\ 0 & \cos\phi & -\sin\phi \\ 0 & \frac{\sin\phi}{\cos\theta} & \frac{\cos\phi}{\cos\theta} \end{pmatrix} \begin{pmatrix} p \\ q \\ r \end{pmatrix} \tag{5}$$

Finally, if the flight path angle $\gamma$ is to be used in the set of variables, the following relation, extracted from [19], is used:

$$\sin\gamma = \cos\alpha\cos\beta\sin\theta - \sin\beta\sin\phi\cos\theta - \sin\alpha\cos\beta\cos\phi\cos\theta \tag{6}$$

The presented flight equations are going to be used to find the stall speed $V_{SR}$. How this speed is defined will be discussed later, but an initial definition would be the minimum speed at which the aircraft can be trimmed. This already allows to introduce several simplifications. First, a stationary flight can be assumed, and therefore $(\dot{u}, \dot{v}, \dot{w}, p, q, r = 0)$. Equations in 5 can now be dismissed. Since thrust (and its coupled effects in lift and drag) is symmetric, the longitudinal and lateral movements can also be decoupled, zeroing all the lateral variables $(\beta, p, r, \phi, \delta_a, \delta_R = 0)$. The second equation from 1, and the first and third from 2 can therefore be dismissed. The problem could also be simplified by assuming horizontal rectilinear $(\gamma = 0)$, or this variable could be left undecided for the moment. For a system of equations, a unique solution exists when the number of equations $(N_e)$ plus the number of constraints $(N_c)$ equals the number of variables, composed by the flight variables $(n_x)$ and the control vector $(n_u)$:

$$N_e + N_c = n_x + n_u \tag{7}$$

Since the problem is comprised in the longitudinal plane, the set of variables is $\boldsymbol{x} = (u, w, \theta, \gamma)^T$ or also $\boldsymbol{x} = (V, \alpha, \theta, \gamma)^T$ after the transformations of 4, so $N_x = 4$. The flight path angle $\gamma$ is introduced together with equation 6. The control surfaces deflections are just formed by the elevator deflection ($\delta_e$). Finally, if the thrust setting of the HLPs is included in the control vector $\boldsymbol{\delta_x} = (\delta_{x_1}, ..., \delta_{x_i}, ..., \delta_{x_N})^T$, there will be just an additional variable if all propellers are equal and there is no differential thrust. This makes $\boldsymbol{u} = (\delta_e, \delta_x)$ making a total amount of unknowns $N_x + N_u + 1 = 6$. The set of equations is the first and third force equations of system 1, the second equation of system 2, expressing the pitch moment equation around the axis $y_b$, and the additional equation 6 that links $\theta$, $\alpha$, and $\gamma$, hence $N_e = 4$. These equations are written:

$$0 = -mg \sin\theta + F_{T,xb} + \frac{1}{2}\rho V^2 S_w (C_L \sin\alpha - C_D \cos\alpha) \tag{8}$$

$$0 = mg \cos\theta + F_{T,zb} - \frac{1}{2}\rho V^2 S_w (C_L \cos\alpha + C_D \sin\alpha) \tag{9}$$

$$0 = \frac{1}{2}\rho V^2 S_w c C_{mA} + M_{T,yb} \tag{10}$$

$$0 = \alpha + \gamma - \theta \tag{11}$$

Even in the most simplified case, imposing horizontal flight and hence the constraint $\gamma = 0$ ($N_c = 1$), and uniform HLPs installation parameters (as in the conventional aircraft version), the problem is still under determined by 1 equation. In any case, since the architecture of the propellers is going to be varied, the thrust will vary across them, and therefore the number of additional variables will be equal to the number of engines, so $N_x + N_u + N_p = 5 + N_p$ if $\gamma \neq 0$. In both cases (uniform and non-uniform HLP geometry), the problem can be transformed into a constrained optimization problem. How these problems have been solved is explained in sections IV and V.

### B. Aerodynamic database

The analysis of the aero-propulsive coupling inside an iterative design is a problematic question. The combined effects of blowing onto a wing with flaps deployed, the consequences for the flow around the tail, and the implications for the trim of the aircraft need to be well captured. All these effects have to be re-computed for any geometry change within the iterative design. Meanwhile, sufficient fidelity that holds the analyses valid for a preliminary phase is required. A compromise between accuracy and computation time is therefore needed.

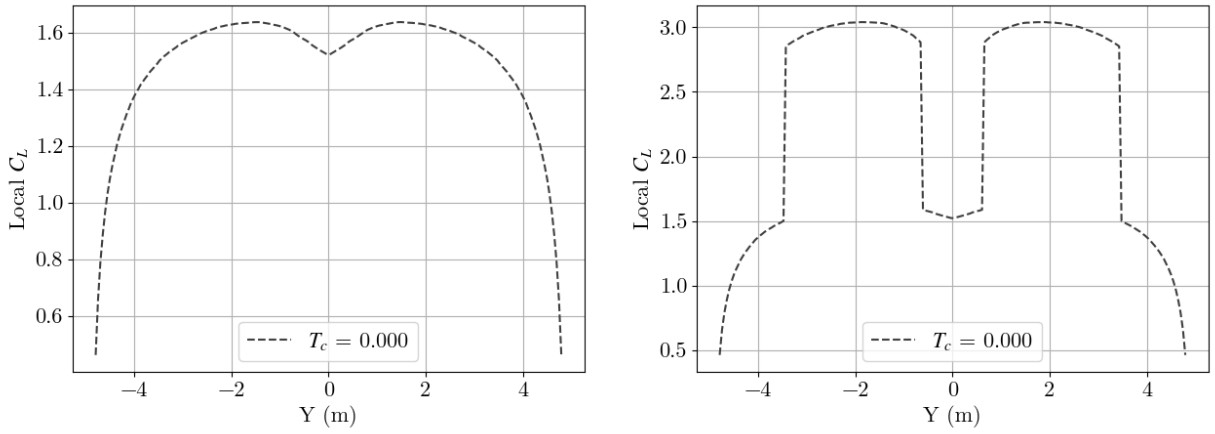


**Fig. 1 Lift distribution $C_L(y)$ for a clean configuration (left) and with the flap deployed (right), in a generic flight situation.**

Consequently, a modified-VLM approach is chosen. A pre-generated aerodynamic database is produced with OpenVSP [17], a mid-fidelity aerodynamic software. The stability derivatives of the aircraft and the lift distribution over the wing are retrieved. The lift distribution is modified with an actuator-disk-based method proposed by Patterson et al. [8]. The method has been modified to account for the effects of flaps. An input to the method is the local speed

induced by the propeller. This speed is estimated from the propeller's thrust by using momentum theory. Specifically, the model described by McCormick is used [20]. The stall characteristics of both the clean and flapped airfoil and the zero-lift line change due to the flap are predicted using XFOIL [21], and are let to propagate into the model. The augmented lift distribution is used as an input for a modified-lifting line theory [22], that computed the induced drag distribution. The wash drag due to the slipstream and the augmented friction drag are added to account for the total drag. Regarding the trimming of the aircraft, to estimate the effects of the slipstream over the tail, a method proposed by Obert et al. [23],[15] is used. The method allows to estimate the performance of the tail under the disturbed downwash.

While accounting for propeller geometry and installation-related variables, the original VLM aerodynamic database does not need to be recalculated when varying any of them. The resultant model is therefore both flexible and extremely low time-consuming. The whole method is built and assembled within a module in Python. Figure 1 shows the clean lift distribution, and the resultant lift distribution when deploying the flap to 30 °, respectively. Note that both the augmentation of lift due to the flap and to the aero-propulsive interaction are done locally, over the affected span stations, influencing the results. This fact will be discussed later. A scheme of the whole aerodynamic model and of the 6 DOF implementation can be seen in figure 10, embedded in the MDO loop. The reader is referred to [7], [5], and [24] for further information of the module.

### C. Reference Aircraft

The proposed method is generic and valid for any DEP configuration given the required inputs, i.e., a VLM analysis, the lift distribution, the airfoil and flap analyses, and the propeller's thrust (so propulsion shall be modeled). The chosen aircraft for all the presented results is NASA's X-57 Maxwell. It is chosen since it is a DEP demonstrator with several inner propellers specifically designed and meant to act as HLPs. Moreover, the modeling relies on a method presented by Patterson, developed for a quick estimation of augmented lift capacities during the design of the X-57. The general characteristics of the X-57 are listed in table 1.

The X-57 geometry used for the analyses, shown in figure 2 is available at the OpenVSP Hangar *. The geometry corresponds to the X-57 Maxwell MOD IV. It is simplified by removing all the engine's (HLP and cruise) propellers, spinners, nacelles, pylons, and the landing gear pod. The airfoil and flap geometry are available at [25].

**Table 1 X-57 general characteristics**

| Parameter | Value |
|---|---|
| Wingspan: $b$ (m) | 9.642 |
| Wing surface: $S_w$ ($m^2$) | 6.196 |
| Overall Length (m) | 8.75 |
| Mass: $m$ (Kg) | 1360 |
| Mean aerodynamic chord: $c$ (m) | 0.649 |
| Ref. cruise speed (m/s) | 77 |
| HLP power (kW) | 10.5 |
| Cruise Propeller power (kW) | 60.08 |
| Horizontal Tailplane area ($m^2$) | 2.452 |
| Vertical Tailplane area ($m^2$) | 3.902 |
| Number of HLPs: $N_p$ | 12 |
| HLPs installation angle: $i_p$ (°) | 0 |
| HLPs Diameter: $D_p$ (m) | 0.5758 |
| Propeller offset: $x_p$ (m) | 0.254 |

*https://hangar.openvsp.org/vspfiles/414

**D. Propulsion modeling**

The original HLPs in the X-57 are designed to achieve a specific and uniform through-the-blade induced axial speed at the desired stall speed condition, at 58 knots. For computing the thrust of each propeller in different flight conditions, the data presented in [26] are used for building the propellers thrust and power coefficients versus the advance ratio charts: $C_T = C_T(J)$ and $C_P = C_P(J)$. The total maximum power of the set of HLPs is ($P = 12 \times 10.5\,kW = 126\,kW$, see table 1). For a given airspeed $V$ and a propeller thrust setting $\delta_{x,i}$, the propeller angular speed $n$ is computed through iteration between the amount of available power and the propeller power coefficient chart :

$$P_i = \frac{P}{N_p}\,\delta_{x,i} = \rho\, n^3\, D_p^5\, C_P\,(J) \tag{12}$$

Once $n$ has been found, the thrust can be computed with $C_T\,(J)$. The propellers are assumed to be mounted with an installation angle $i_p$ with respect to the aircraft's X body axis. The propeller's normal forces and moments are neglected, given the reduced propeller's solidity and thrust coefficient when distributing the power and thrust across a larger propeller area [7]. The thrust force and moment are computed by adding the individual contribution of each engine:

$$\mathbf{F}_{T_B} = \begin{pmatrix} \sum_{i=1}^{N} T_i \cos i_p \\ 0 \\ \sum_{i=1}^{N} T_i \sin i_p \end{pmatrix}, \qquad \mathbf{M}_{T_B} = \begin{pmatrix} \sum_{i=1}^{N} T_i y_i \sin i_p \\ \sum_{i=1}^{N} T_i (z_i \cos i_p - x_i \sin i_p) \\ \sum_{i=1}^{N} -T_i y_i \cos i_p \end{pmatrix} \tag{13}$$

where $T_i$ is the thrust produced by the $i^{th}$ propeller, located in $\boldsymbol{x_i} = (x_i, y_i, z_i)^T$ in the body X-axis, with throttle command $\delta_{x_i}$.

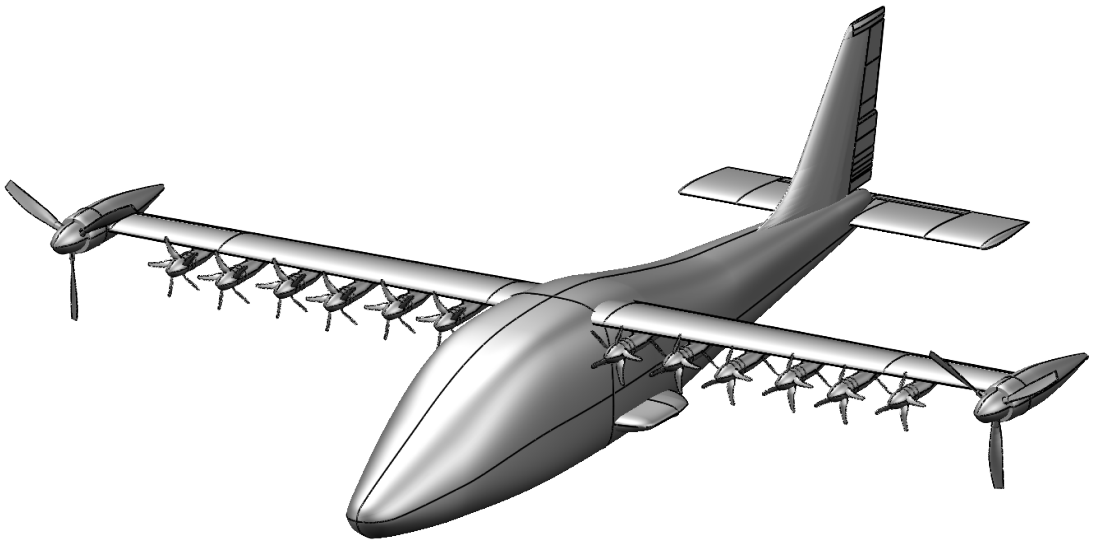

**Fig. 2 X-57 geometry for OpenVSP**

### E. Modeling Validation

Regarding the validation of the model, this work relays on two published analyses. The first one is a computational analysis of the aerodynamics of the unpowered X-57 Mod-III [27], meaning that both high lift and cruise propulsors are inoperative during the analysis. The second is a computational analysis of the Mod-IV including the HLP propulsors and, therefore, the aero-propulsive interaction, together with flap deflection [28]. A Reynolds-averaged Navier Stokes method implemented in LAVA (Launch Ascent and Vehicle Aerodynamics), is used in both analyses to compute the results. The two evaluated and compared flight cases are shown in table 2, and the results are compared in figure 3.

**Table 2 Flight cases validated**

| Condition | Altitude (m) | Mach | Thrust setting (%) | Flaps (°) |
|---|---|---|---|---|
| 1 | ≃ 750 | 0.149 | 0 | 10 |
| 2 | ≃ 750 | 0.119 | 39 | 30 |

Results are in line with expectations given the level of fidelity of the methods implemented. The analysis effectively estimates complex cases with flap deflection and/or blowing. In the linear pre-stall region, the $C_L$ is estimated within an error of approximately 5%, and the $C_D$ around 10%. The stall point is also accurately predicted, whether it is more abrupt (case 2) or progressive (case 1). However, post-stall drag estimation is challenging. In the proposed model, drag increases rapidly and diverges from the CFD computations. Nevertheless, this guarantees that the aircraft will not be trimmed if the boundary layer has begun to detach, so the model is considered valid for the intended purpose. Again, the biggest asset is the computational cost needed to evaluate different configurations and flight conditions, in the order of seconds.

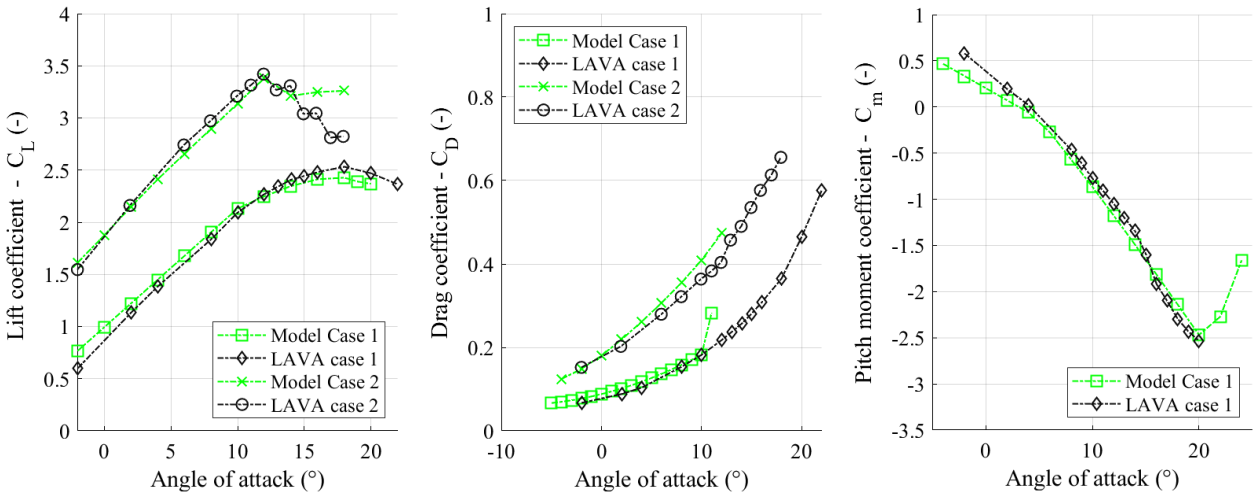


**Fig. 3 Comparison of results between [28] and [27] and the proposed modeling, for the lift $C_L$, drag $C_D$, and pitch moment $C_m$ coefficients.**

## III. Problem approach: Sensitivity Analysis

The following section is focused on the amount of potential lift that can be achieved through the aero-propulsive coupling when varying the propeller's diameter, different installation variables such as the propeller tilt angle and the offset to the wing's leading edge, and the number of propellers. It introduces as well some of the general constraints and hypotheses made for the later MDO. The aircraft is not trimmed in the following analyses. Therefore, the analyses are conducted at an imposed flight condition, presented in table 3. These conditions are the ones of the aimed stall speed of the X-57, except for the flap, which is not deployed here. Regarding the propellers and some relevant installation parameters, the nominal values for the aircraft are gathered in table 1.

**Table 3 Flight conditions**

| **Airspeed (m/s)** | **Altitude (m)** | **Thrust setting** (%) | **Angle of attack** (°) | **Flaps** (°) |
|---|---|---|---|---|
| 28.3 | 0 | 100 | 8 | 0 |

### A. Assumptions

To render realistic the analysis, some assumptions and constraints are made:

- As explained previously, the original HLPs aimed to achieve a specific, uniform induced axial speed at the desired stall speed condition. When varying the diameter of a propeller the same design is kept (i.e., chord distribution, twist distribution, blade's airfoil, etc.). This will hence change the operating point in the $C_T = C_T(J)$ and $C_P = C_P(J)$ charts. The propeller will maintain the uniform axial speed design but for a different induced speed.
- Whichever number of HLPs is evaluated, the total maximum power available remains constant and equal to the one in the conventional version, i.e., $P_{max} = 12x10.5\ kW$.
- The propeller angular speed is limited so that the Mach at the blade tip cannot be higher than $M = 0.5$. This is the Mach achieved in the conventional version, at the same conditions, with the maximum theoretical rpm of the propeller. For a given supplied power the angular speed will grow with the airspeed, but with such a restrictive limitation it is ensured that propellers will be kept far from the transonic region also at off-design conditions.
- Propellers cannot be superposed, so the same area is not blown by two different propellers.

### B. Results

Figures 4 and 5 show the effects on the wing lift coefficient $C_{L,w}$ when varying the propellers installation angle $i_p$ and their offset distance $x_p$ to the wing, behaving accordingly to [11] and [9]. Reducing $i_p$ leads to higher lift coefficients since it modifies the apparent angle of attack of the sections behind the propeller. On the other hand, an increase in $x_p$ allows for further contraction of the slipstream, blowing the wing with a higher speed. Although a lot of lift augmentation can be obtained through these two mechanisms, they also lead to undesired effects. Larger or tilted nacelles will increase both the drag and the weight and will cause unwanted structural effects. Finally, not only the potential to delay stall is lost if the propeller axis is not aligned with the freestream, but the augmentation of the apparent angle of attack due to large negatives $i_p$ can produce the early stall of some regions of the wing (in the case analyzed, stall begins at around $i_p = 15$ ° for $\alpha = 8$ °).

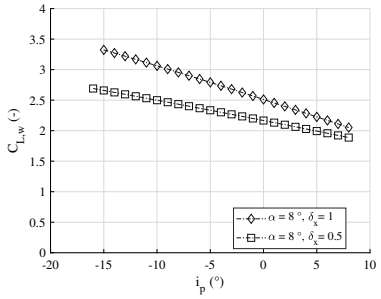


**Fig. 4** $i_p$ **vs** $C_{L,w}$

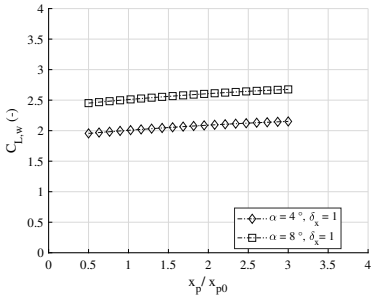


**Fig. 5** $x_p$ **vs** $C_{L,w}$

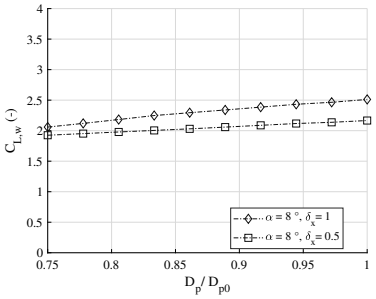


**Fig. 6** $D_p$ **vs** $C_{L,w}$

Figure 6, in turn, shows the effect of varying the diameter of the propellers for the conventional configuration, without moving their span position. Since total power is being kept constant, decreasing the diameter leads to higher induced axial speeds, but less wing is being blown, so $C_{L,w}$ is reduced.

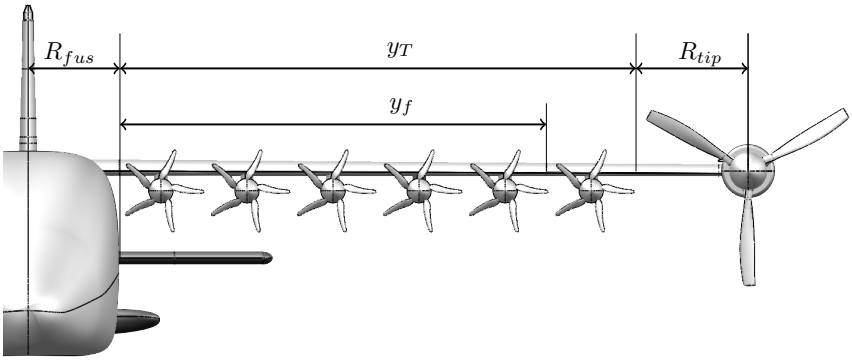


**Fig. 7 Front view of the X-57**

Figure 8 plots the wing lift coefficient $C_{L,w}$ for several different configurations of the number of propellers and their diameters, under the conditions in table 3. For all numbers of propellers, $D_p^*$, (or $D_p/D_p^* = 1$) represents the propeller diameter for having all the available wing span blown $y_T$, see figure 7. The propeller diameter $D_p^*$ can be easily calculated as $D_p^* = \frac{\frac{b}{2} - R_{fus} - R_{tip}}{N_p/2}$, where $R_{fus}$ is the maximum fuselage width and $R_{tip}$ is the radius of the cruise propeller installed in the wing tip. For these cases, the position of the propellers is fixed due to this constraint. For the reduced diameters $D_p/D_p^* < 1$, since this condition frees some available wingspan, the propellers are all moved toward the wing root, while respecting the no-superposition constraint. This is beneficial due to the natural lift distribution on the wing and because of the position of the flap (although flaps are not deployed here), see figure 7.

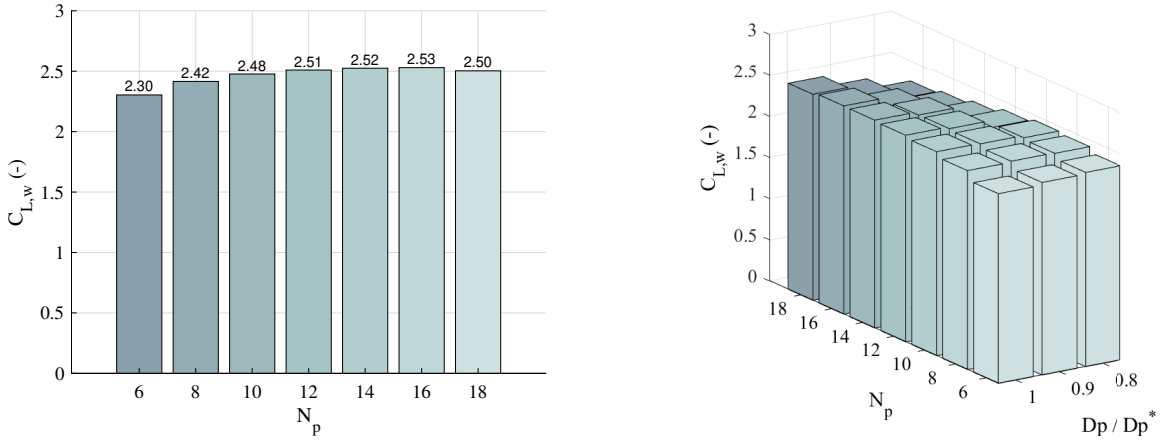


**Fig. 8 $C_{L,w}$ for several configurations**

Table 4 presents the results for each configuration analyzed. The configuration with 16 propellers and the wing fully embedded in the slipstream shows the highest wing lift coefficient. When reducing the prop's diameter and moving them closer to the fuselage, there are only benefits for the last two configurations with 8 and 6 props, which are marked with an asterisk if this is the case. It is important to note that this analysis only focuses on the lift generated through aero-propulsive coupling, however, other variables play a more important role in the HLPs-configuration decision [8]. Across all configurations, the $C_{L,w}$ values are very close, as long as the installed power and the blown area remain constant. One interesting factor to look at is thrust. In a conventional aircraft, propellers are idle during descent, and flaps create the necessary drag to slow the aircraft down. If HLPs are to be used during descent to increase $C_{L,max}$, the

minimum possible amount of thrust will make it easier to control the descent at the desired speed. Notably, there are significant differences in total thrust. Increasing the number of propellers leads to lower total thrust, but the blade tip is quickly limited due to transonic speeds. On the other hand, reducing the number of propellers simplifies the design but leads to higher thrusts and thrust-per-engine, rendering the aircraft more sensitive to engine failure.

**Table 4 Propulsion analysis for each configuration**

| **Configuration:** $N_p$ | $D_p$ **(m)** | $C_{L,w}$ **(-)** | **Thrust per prop** $T_i$ **(N)** | **Total thrust** $T$ **(N)** |
|---|---|---|---|---|
| 18 | 0.384 | 2.49 | 137.0 | 2465 |
| 16 | 0.432 | 2.53 | 164.9 | 2637 |
| 14 | 0.494 | 2.52 | 193.9 | 2715 |
| 12 | 0.576 | 2.50 | 233.5 | 2802 |
| 10 | 0.941 | 2.47 | 290.4 | 2904 |
| 8 | 0.864 | 2.41 | 378.3 | 3026 |
| 6 | 1.152 | 2.3 | 529.3 | 3176 |
| 8* | 0.778 | 2.43 | 362.3 | 2898 |
| 6* | 0.922 | 2.36 | 487.8 | 2927 |

***: Configurations where propellers have been stacked around the wing root.**

Since the analysis conducted has been done without trimming the aircraft, the configurations with more lift are not necessarily the ones able to achieve a lower stall speed $V_{SR}$. Configurations with higher thrust could eventually be able to achieve higher angles of attack since they could counter more drag, and therefore achieve higher lift coefficients. Finally, this could also depend on the capacity of the aircraft of countering the large nose-down pitch moment that will eventually appear due to the high thrust settings and the high angles of attack. In the following section the aircraft will be trimmed to estimate the potential stall speed $V_{SR}$ of the conventional version of the aircraft.

## IV. Stall speed

The previous section studied the effects of the installation characteristics on the lift generated through the aero-propulsive interaction, without trimming the aircraft. The following section presents the results from the computation of the stall speed of the original X-57. The stall speed is calculated through constrained minimization to find the minimum speed of the aircraft in a trimmed condition while taking into account the effects of the aero-propulsive coupling.

### A. Finding the stall speed by minimization

The aim is to calculate the stall speed $V_{SR}$ of the original X-57 aircraft. The stall speed for GA aircraft is defined by the regulation, whether from Federal Aviation Regulations (FARs) or Certification Specifications for Normal Category Aeroplanes (CS-23), and a series of conditions for its determination are stated. These conditions do not allow currently any credit from blowing from HLPs. Specifically, the CS-23 says that it shall be determined with "Engines idling, or, if that resultant thrust causes an appreciable decrease in stall speed, not more than zero thrust at the stall speed". A DEP aircraft using HLPs to augment lift and reduce the stall speed cannot be, therefore, certified under current regulations. However, establishing a regulation for $V_{SR}$ of DEP aircraft working with HLPs is out of the scope of this paper. To simplify the analysis, the stall speed $V_{SR}$ is defined here as the minimum speed at which the aircraft can be trimmed, with zero flight path angle $\gamma$, flaps deployed, with the high lift propellers operating to enhance the lift of the aircraft, at the nominal weight and at sea level. To trim the aircraft, as explained in subsection II.A, the system of equations formed by 8, needs to be solved. However, as mentioned before, the unknowns outnumber the equations. These equations can be simplified with the assumption of horizontal flight ($\gamma = 0$), but the problem is, however, still under-determined by one equation.

In order to find the stall speed of the aircraft, the problem can be posed as a constrained optimization. The cost function is the flight speed, defined with the lift equation. The set of constraints is the aforementioned equations to trim the aircraft, with the simplifying assumptions. Note that the lift equation is present in both the cost function and the constraints. This is done since the trim needs to be forced with a constraint to be satisfactory. Although the assumption

$\gamma = 0$ is done, it is still written as a variable, without modifying the problem since the equation linking $\alpha$, $\theta$, and $\gamma$ is still kept. Upper and lower bound, presented in table 5 are added on the variables $\tilde{x}$, in order to keep the optimization within the feasible region. For implementing the optimization algorithm a Sequential Least Squares Programming algorithm, from the Python library SciPy, is chosen [29].

Thus, the problem is written as:

$$\min_{\tilde{x}} \quad V = \sqrt{\frac{mg\cos\theta - \sum_{i=1}^{N} C_{T,i}\sin i_p}{\frac{1}{2}\rho S_w \ (C_L\cos\alpha + C_D\sin\alpha)}} \tag{14}$$

$$\text{With:} \quad \tilde{x} = [\alpha, \theta, V, \gamma, \delta_e, \delta_x]^T \tag{15}$$

Subjected to:

$$0 = -\frac{2mg}{\rho V^2 S_w}\sin\theta + \sum_{i=1}^{N_p} C_{T,i}\cos i_p + C_L\sin\alpha - C_D\cos\alpha \tag{16}$$

$$0 = \frac{2mg}{\rho V^2 S_w}\cos\theta - \sum_{i=1}^{N_p} C_{T,i}\sin i_p - C_L\cos\alpha - C_D\sin\alpha \tag{17}$$

$$0 = C_{mA} - \sum_{i=1}^{N_p} C_{T,i}(\hat{z_i}\cos i_p - \hat{x_i}\sin i_p) \tag{18}$$

$$0 = \alpha + \gamma - \theta \tag{19}$$

**Table 5 Variables bounds**

| Variable | Bounds |
|---|---|
| Airspeed $V$ (m/s) | $20 < V < 40$ |
| Angle of attack $\alpha$ (°) | $-5 < \alpha < 25$ |
| Elevator $\delta_e$ (°) | $-40 < \delta_e < 40$ |
| Thrust setting $\delta_x$ (%) | $0 < \delta_x < 100$ |

The results are presented in tables 6.a and 6.b. A distinction has been done depending on the imposed lower bound on the elevator deflection. An explanation should be given now about the trimming results of the aircraft. The X-57 has an elevator that occupies a small fraction of the horizontal tail. To fly at low airspeeds, high angles of attack are required to generate more lift. This results in increased negative nose-down pitch moments. In addition, by deploying the flaps and blowing onto the wing, the lift application point on the wing is usually moved backward, emphasizing this effect. The most important contribution is, however, the pitch moment created by the propeller's thrust. The HLPs in the X-57 are positioned around 0.45 m above the aircraft's center of gravity, which results in a considerable nose-down pitch moment if high thrust settings are used. Consequently, a large negative deflection of the elevator is necessary to counter this moment. The elevator has an efficiency limit (typically around -30 °) beyond which the airflow would detach, and the efficiency of the elevator would be reduced to zero. If this lower bound is set on the elevator deflection, then this is the limiting factor that prevents flying at a lower speed. The thrust setting will therefore not be the maximum. It is important also to stress that the pilot will no longer have pitch control on the aircraft since the elevator is saturated.

**Table 6.a Stall speed with bounded elevator**

| Variable | Value |
|---|---|
| Stall speed $V_{SR}$ (m/s) | 29.42 |
| Angle of attack $\alpha$ (°) | 9.04 |
| Elevator $\delta_e$ (°) | -30 |
| Thrust setting $\delta_x$ (%) | 95.0 |
| Thrust $T$ (N) | 2635 |
| Lift Coefficient $C_L$ (-) | 3.94 |
| Drag Coefficient $C_D$ (-) | 0.79 |
| Pitch moment Coefficient $C_m$ (-) | 0.56 |

**Table 6.b Stall speed with elevator unbounded**

| Variable | Value |
|---|---|
| Stall speed $V_{SR}$ (m/s) | 28.75 |
| Angle of attack $\alpha$ (°) | 9.58 |
| Elevator $\delta_e$ (°) | -32.6 |
| Thrust setting $\delta_x$ (%) | 100 |
| Thrust $T$ (N) | 2773 |
| Lift Coefficient $C_L$ (-) | 4.10 |
| Drag Coefficient $C_D$ (-) | 0.87 |
| Pitch moment Coefficient $C_m$ (-) | 0.62 |

On the other hand, if no bound is set on the elevator, then the limiting factor for the stall speed is the thrust. If the elevator deflection resulting from the trim is not highly unrealistic (but above the aforementioned limit), the pitch moment created by this deflection could potentially be produced with a trim stab or a deflective horizontal tail. This would allow achieving the minimum stall speed with full thrust even if the elevator is saturated at the marked 30 ° limit.

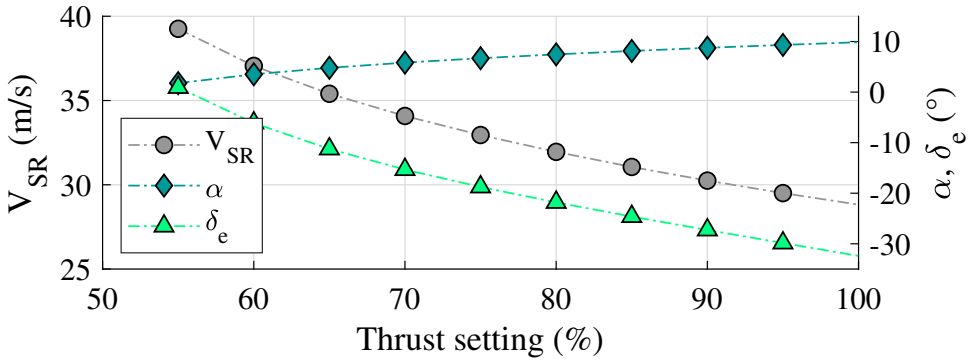


**Fig. 9 Stall speed $V_{SR}$, angle of attack $\alpha$ and elevator deflection $\delta_e$ versus the thrust setting $\delta_x$, for the aircraft trimmed.**

Finally, figure 9 shows the value of the stall speed $V_{SR}$, the angle of attack $\alpha$ and the elevator deflection $\delta_e$ with the aircraft trimmed, for different levels of the thrust setting $\delta_x$, and for zero flight path angle $\gamma = 0$. As expected, increasing the thrust setting $\delta_x$ results in lower stall speeds for the aircraft, due to two reasons. First, lift is enhanced due to the increased blowing onto the wing, and second, higher angles of attacks are reachable (in fact required) for compensating the thrust, producing more lift. The moment due to thrust obliges, however, to set high negative deflections of the elevator. As thrust drops, less blowing is produced and the angle of attack is forced to reduce, so the drag can be countered by the thrust. This also leads to higher stall speeds and alleviates the elevator control. If the aircraft is to be trimmed for thrust settings $\delta_x$ of the HLPs under the 55%, the cruise propellers of the X-57 need to be turned on, otherwise, the aircraft will not keep the horizontal flight with $\gamma = 0$.

As a reminder, the X-57 aims to achieve a stall speed of 58 knots (29.8 m/s). Being the gross weight of 3000 lb = 1360 kg, this means that the $C_{L,max}$ should be around 3.95. Therefore, the obtained results are acceptable and provide confidence to proceed with the optimization process.

# V. Optimization

The stall speed of the original X-57 has been calculated in section IV, and a sensitivity analysis was performed in section III to study the effects on the aero-propulsive coupling of propeller-geometry and installation modifications. The following section will address the multidisciplinary optimization through the iterative design of the propeller installation parameters.

The considered MDO will address two main design objectives $\boldsymbol{f}$. The first one will be the minimization of the stall speed $V_{SR}$. The stall speed is intended to be minimized while keeping the aircraft trimmed, forcing to set up a constrained optimization. The set of constraints $\boldsymbol{g}$ will be discussed later, but the equations presented in subsection II.A and used in section IV will be utilized. The second objective function will be the reduction of the power $P$ of the HLPs. To render fair the minimization, the aircraft should be able to be trimmed at the same stall speed $V_{SR}$ achieved by the conventional version. Additional constraints are added to keep realistic the analysis and will be discussed later.

Figure 10 presents the extended design structure matrix of the multidisciplinary optimization problem. The optimizer chosen is once again the Sequential Least Squares Programming algorithm from the Python library SciPy. The optimization algorithm feeds the design vector $\boldsymbol{x}$ to the different modules. The different variables contained in $\boldsymbol{x}$ are discussed later. As explained, modules 1 and 2 are not iterated, and are used to compute the wing (and aircraft) and airfoil aerodynamic database. This database is later, together with the outcome from the propulsion module 3, used by the aero-propulsive coupling method and the horizontal tail performance module. The first one calculates the augmented lift and drag coefficients on the wing due to the propeller slipstream. The second one is in charge of determining the disturbed downwash and the slipstream position with respect to the tail, to estimate its performance. Finally, aerodynamic forces and moments are used for the calculation of the cost function and the constraints, and fed back to the optimizer.

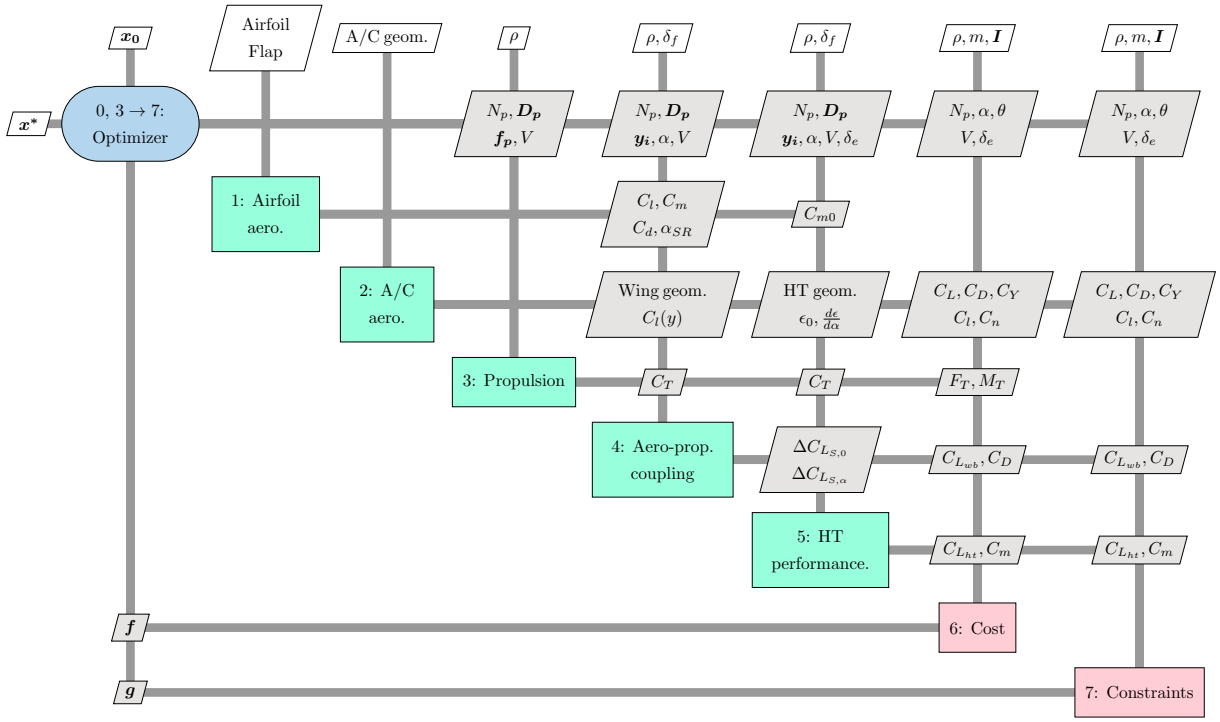


**Fig. 10 Extended design structure matrix of multidisciplinary design optimization setup.**

The magnitudes $\epsilon_0$ and $\frac{d\epsilon}{d\alpha}$ stand for the downwash zero angle and the downwash derivative, which are calculated with the VLM. Magnitudes $\Delta C_{L_{S,0}}$ and $\Delta C_{L_{S,\alpha}}$ are required for the slipstream determination method and stand for the change in the wing lift coefficient at zero angle of attack and at the given angle of attack, between a configuration without propeller slipstream $C_T = 0$, and a configuration with it. The rest of the magnitudes are defined either in the nomenclature or inside the optimization problem definition.

## Minimization of the stall speed $V_{SR}$

### A. Optimization Problem Definition

The problem consists in the search of an installation configuration for the propellers leading to a reduction of the stall speed throughout the creation of more aero-propulsive-resultant lift. Since the local flow conditions and the lift distribution vary across the wingspan, is it reasonable to expect that there will exist an optimal design other than equal installation parameters for all the propellers [9]. Essentially, by achieving a higher $C_{L,max}$, there will be room for an eventual reduction of the wing surface, and therefore for a more-optimal cruise design. The installation parameters varied are presented in table 8.

**Table 8 Installation parameters varied during the optimization**

| Variable | Concept | Form |
|---|---|---|
| $\boldsymbol{N_p}$ | Number of propellers | $\boldsymbol{N_p} = (6, 8, 10, 12, 14, 16, 18)^T$ |
| $\boldsymbol{D_p}$ (m) | Diameter of the propellers | $\boldsymbol{D_p} = (D_{p,1}, D_{p,2}, ..., D_{p,N_p/2})^T \in \Re^{N_p/2}$ |
| $\boldsymbol{f_p}$ (-) | Power fraction of the propellers | $\boldsymbol{f_p} = (f_{p,1}, f_{p,2}, ..., f_{p,N_p/2})^T \in \Re^{N_p/2}$ |

Since $\boldsymbol{N_p}$ is the only discrete variable, an optimization for each number of propellers is performed. A symmetric configuration is assumed for both semi-wings, so the size of $\boldsymbol{D_p}$ and $\boldsymbol{f_p}$ vectors is equal to half the number of propellers in the current iteration, $N_p/2$. The order of these installation vectors is so that the first element corresponds to the propeller closer to the wing tip, while the last element corresponds to the propeller closer to the fuselage. The position of the $i^{th}$ propeller is therefore fixed by the equation:

$$y_i = R_{fus} + 0.5D_{p,N_p/2} + \sum_{j=0}^{j=N_p/2-i-1} (0.5D_{p,N_p/2-j} + 0.5D_{p,N_p/2-j-1}) \tag{20}$$

This respects the assumption made in III that states that propellers cannot be superposed, and at the same time, leaves no free space between the propellers, washing the entire wing area between the first and the last propeller. The last propeller $(N_p/2)^{th}$ is as close as possible to the fuselage due to the observations done in III where this was beneficial. Finally, $\boldsymbol{f_p}$ is the vector containing the power fraction of each propeller, with respect to the total available power (126 $kW$, see 1). The problem is therefore written as:

$$\min_{\tilde{x}} \; V = \sqrt{\frac{mg\cos\theta - \sum_{i=1}^{N} C_{T,i}\sin i_p}{\frac{1}{2}\rho S_w \, (C_L\cos\alpha + C_D\sin\alpha)}}$$

$$\text{With:} \quad \tilde{x} = [\alpha, \theta, V, \gamma, \delta_e]^T + \boldsymbol{D_p} + \boldsymbol{f_p}$$

Subjected to:

$$g_1 = \begin{cases} 0 = -\frac{2mg}{\rho V^2 S_w}\sin\theta + \sum_{i=1}^{N_p} C_{T,i}\cos i_p + C_L\sin\alpha - C_D\cos\alpha \\ 0 = \frac{2mg}{\rho V^2 S_w}\cos\theta - \sum_{i=1}^{N_p} C_{T,i}\sin i_p - C_L\cos\alpha - C_D\sin\alpha \\ 0 = C_{mA} - \sum_{i=1}^{N_p} C_{T,i}(\hat{z}_i\cos i_p - \hat{x}_i\sin i_p) \\ 0 = \alpha + \gamma - \theta \end{cases} \tag{21}$$

$$g_2 = \begin{cases} 0 < (0.5b - R_{tip}) - (\sum_{i=1}^{N_p/2} D_p + R_{fus}) \\ 0 < 0.5 - \sum_{i=1}^{N_p/2} P_p \\ \forall D_{p,i} : n < n_{max}, \;\; n_{max} = \; n : \;\; M = 0.5 \end{cases} \tag{22}$$

For $N_p = 6, 8, 10, 12, 14, 16, 18$

In addition to the first set of equality constraints ($g_1$), imposed to find the minimum speed with the aircraft trimmed, a second set of inequality constraints ($g_2$) is added. These ensure that the addition of the diameters of the propellers on one semi-wing is within the available space (see figure 7); that the maximum power is not surpassed; and that the angular speed of any propeller is not bigger than the one that would cause $M = 0.5$ in the tip of the blade at the given speed and diameter and for a conservative induced speed factor of 0.8, similarly to what was done in section III.

The weight is not penalized when varying the number of propellers. Since the total power is kept constant, and following the reasoning in [8], there is no change in the weight of the motors, and similar reasoning is done with the weight of the nacelles. Again, lower and upper bounds are selected for the variables of the problem, in particular:

**Table 9 Variables bounds**

| Variable | Bounds |
|---|---|
| Airspeed $V$ (m/s) | $20 < V < 40$ |
| Angle of attack $\alpha$ (°) | $-5 < \alpha < 25$ |
| Elevator $\delta_e$ (°) | $-50$ / $-30 < \delta_e < 40$ |
| Propeller diameter $D_{p,i}$ (m) | $0.6D_{p0} < D_{p,i} < 2.5D_{p0}$ |
| Propeller power fraction $f_{p,i}$ (-) | $0.01 < f_{p,i} < 0.5$ |

where $D_{p0}$ represents the original diameter of a propeller in the conventional X-57 version with 12 HLPs. Two different lower bounds are set on the elevator. As previously explained, this can greatly determine the effective minimum speed at which the aircraft can be trimmed. The optimizations are therefore conducted for a lower limit of $\delta_e = -30°$, which represents a usual limit for the deflection of this element, and without a lower bound. As already mentioned, since the pitch moment due to the resultant elevator deflection could potentially be produced with a trim stab or a deflective horizontal tail, the solution is still relevant.

### B. Results

The optimization results for each $N_p$ configuration are presented in figure 11, and detailed in table 10. For configurations with 12 or fewer propellers, two solutions are presented depending on the elevator bound imposed. Configurations above this number of propellers are only limited by the total power $P$.

**Table 10 Stall speed results**

| **Variable** | **($N_p$):** | 6 | 8 | 10 | 12 | 14 | 16 | 18 |
|---|---|---|---|---|---|---|---|---|
| Stall speed $V_{SR}$ (m/s) | | 27.09 / 30.01 | 26.93 / 29.21 | 27.91 / 28.48 | 28.29 / 28.58 | 28.98 | 29.25 | 30.21 |
| Angle of attack $\alpha$ (°) | | 15.62 / 10.6 | 14.5 / 9.9 | 10.3 / 9.6 | 11.2 / 9.7 | 8.9 | 8.83 | 7.1 |
| Elevator $\delta_e$ (°) | | -47.8 / -30 | -44.3 / -30 | -35.7 / -30 | -31.8 / -30 | -28.3 | -27.3 | -24.7 |
| Total thrust $T$ (N) | | 3222 / 2403 | 3137 / 2574 | 2909 / 2732 | 2838 / 2775 | 2721 | 2706 | 2538 |
| Lift Coefficient $C_L$ (-) | | 4.48 / 3.78 | 4.56 / 3.99 | 4.33 / 4.19 | 4.23 / 4.15 | 4.05 | 3.98 | 3.76 |
| Drag Coefficient $C_D$ (-) | | 1.11 / 0.69 | 1.10 / 0.78 | 0.97 / 0.88 | 0.92 / 0.88 | 0.84 | 0.82 | 0.73 |

From both figure 11 and table 10, it can be seen that when no limit is set on the elevator, configurations with fewer propellers are able to achieve reduced stall speeds. When distributing the same amount of power among equally-designed propellers, the configurations with fewer propellers provide higher thrusts. These higher thrusts allow to compensate for more drag and therefore achieve higher angles of attack, leading to lower stall speeds. The propellers in the best configuration with 6 propellers are, however, too big. Under the constraint which keeps maximum power constant, they are unable to produce the same induced speed onto the wing as the best configuration with 8 propellers. This explains the minimum seen in figure 11.

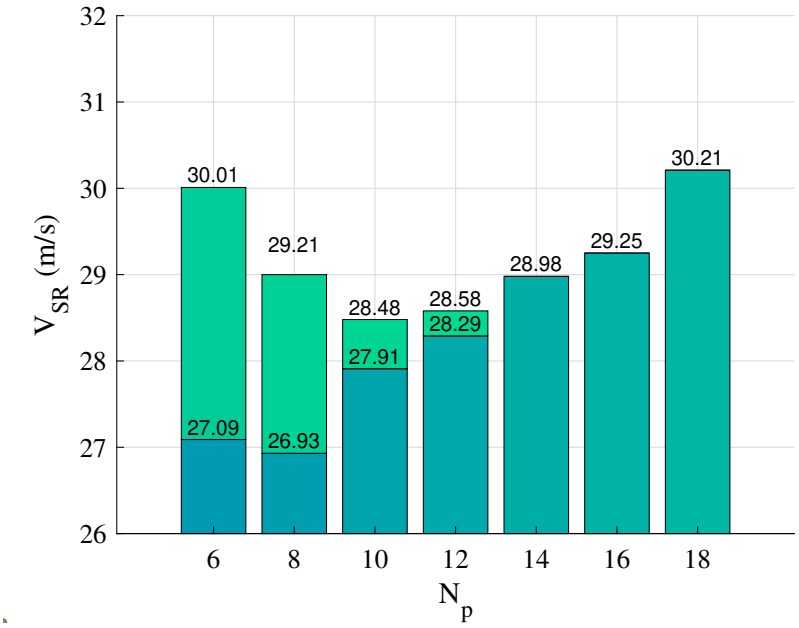


**Fig. 11 Minimum stall speed $V_{SR}$ found for each $N_p$ configuration.**

However, when limiting the elevator to $\delta_e = 30°$, the configurations with 6 and 8 propellers are no longer able to counter both the nose-down aerodynamic and propulsive pitch moments. As a result, the maximum reachable angle of attack is considerably reduced, and less maximum lift coefficient $C_{L,max}$ can be achieved, resulting in higher stall speeds $V_{SR}$.

It is depending on this limit for the elevator, that the configurations with 10 propellers and 8 propellers, respectively, are found to achieve the minimum stall speed $V_{SR}$. For the sake of brevity, the propeller's geometry configuration is only presented for the configurations that achieve the minimum stall speed, in tables 11 and 12.

**Table 11 Winner configuration, without elevator lower bound**

| Variable | Value |
|---|---|
| Number of propellers $N_p$ | 8 |
| Stall speed $V^*_{SR}$ (m/s) | 26.93 |
| Angle of attack $\alpha$ (°) | 14.5 |
| Elevator $\delta_e$ (°) | -44.3 |
| Diameter of the propellers $\boldsymbol{D^*_p}$ (m) | $(0.513, 1.021, 1.232, 0.688)^T$ |
| Power fraction of the propellers $\boldsymbol{f^*_p}$ (-) | $(0.037, 0.161, 0.235, 0.067)^T$ |
| Thrust $T$ (N) | 3137 |
| Lift Coefficient $C_L$ (-) | 4.56 |
| Drag Coefficient $C_D$ (-) | 1.10 |

The configuration with 8 propellers and the geometry described in table 11 achieves a stall speed $V_{SR}$ of 26.93 m/s. When compared with the minimum stall speed achieved by the original X-57 aircraft (28.75 m/s, table 6.b), this results in a reduction of 6.3 %, assuming in both cases that no limit is imposed on the elevator. The deflection of this element is however considerably high, and the moment generated can unrealistically be produced by other means, like a trim tab or a deflective horizontal tail.

Table 12 shows the best configuration geometry found to minimize the stall speed, while restricting the elevator, with 10 propellers. The resultant stall speed is $V_{SR}$ = 28.48 m/s, bringing a reduction of 3.2 % with respect to the stall speed of the conventional version with the elevator bounded (29.42 m/s, table 6.a). The proposed configuration is able

to achieve a higher angle of attack (9.7 ° vs 9.04 °), and a higher maximum lift coefficient $C_{L,max}$ (4.18 vs 3.94), while increasing the total thrust $T$ around 100 N, since all the available power is used. To recall, in the conventional version, the elevator restriction does not allow the use of thrust settings above $\delta_x = 0.95$ (95 %).

**Table 12 Winner configuration with elevator lower bound**

| Variable | Value |
|---|---|
| Number of propellers $N_p$ | 10 |
| Stall speed $V^*_{SR}$ (m/s) | 28.52 |
| Angle of attack $\alpha$ (°) | 9.7 |
| Elevator $\delta_e$ (°) | -30 |
| Diameter of the propellers $\boldsymbol{D^*_p}$ (m) | $(0.587, 0.780, 0.659, 0.570, 0.347)^T$ |
| Power fraction of the propellers $\boldsymbol{f^*_p}$ (-) | $(0.115, 0.170, 0.122, 0.074, 0.019)^T$ |
| Thrust $T$ (N) | 2727 |
| Lift Coefficient $C_L$ (-) | 4.18 |
| Drag Coefficient $C_D$ (-) | 0.87 |

There are two main reasons explaining why the optimized configuration achieves a reduced stall speed. The first one is related to the exploitation of the natural increase of the lift provided by the flap. Optimized configurations tend to distribute all the blowing in the flapped span of the wing. This is shown in figure 12, where all the propellers are kept inside this region, noted $y_f$. Meanwhile, the region of the wing with the aileron $y_{ail}$, towards the wing tip, is kept empty. In the model, the augmentation of lift due to flap deflection is done locally (see figure VI). In reality, lift distribution is smoother, so less improvement can be expected from this effect.

The second reason is related to the optimized configuration's capacity to reach higher angles of attack while using all the available power and at the same time counter the higher resultant nose-down pitch moment. When observing figure 12, it can be seen that the smaller propellers have been positioned in front of the horizontal tail, within the wingspan $y = b_h/2$. To counter the large negative thrust pitch moment, a higher nose-up pitch moment needs to be created in the horizontal tail, through negative lift in this element. The higher the downwash in the tail, the larger the negative lift generated.

According to [23], [30], one of the contributions to the downwash behind a wing with rotating propellers, consists of an inflow from the external flow into the slipstream, noted $\Delta\epsilon$. If the tail is below the slipstream, then $\Delta\epsilon < 0$ (see figure 6 in [30]), and the downwash will be reduced. In the case of the X-57, reducing the diameter of the propellers in front of the tail decreases the importance of the negative term $\Delta\epsilon$, increasing the downwash. As a result, the moment in the tail is more positive, countering the thrust moment. In any case, this highlights the importance of the interaction between the slipstream and the horizontal tail, and how it should be considered during the preliminary design of the aircraft.

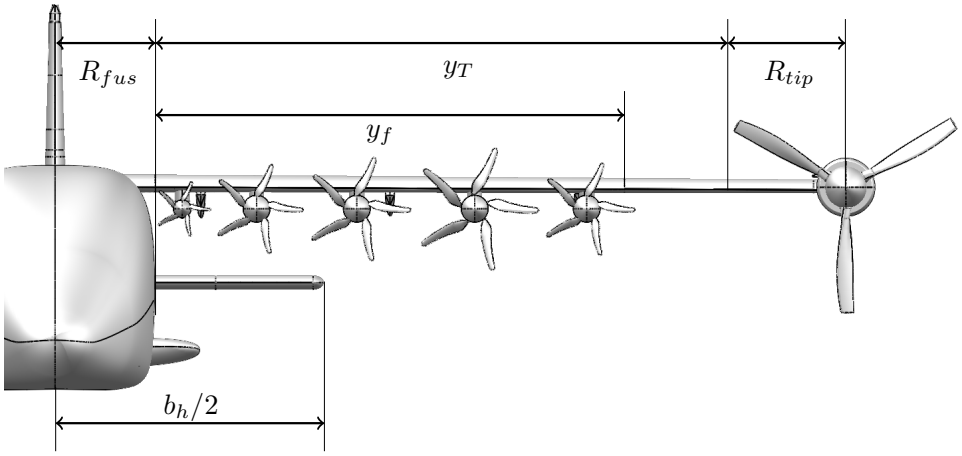


**Fig. 12 Front view of the optimized configuration for $V_{SR}$ with bounded elevator**

## Minimization of the installed power $P$

The optimization carried out in section V highlighted important aspects related to the trimming of the aircraft, the total applied thrust, the emerged pitch moment, and the amount of elevator deflection demanded. A new optimization is now posed, aiming to reduce the total HLPs power used.

### C. Optimization Problem Definition

Distributing the power among fewer propellers leads to higher total thrust. This will generally allow countering more drag and reaching higher angles of attack, as long as the resultant thrust pitch moment can be countered. However, increasing the thrust can also lead to undesired effects. First, in the case of the X-57, the nose-down pitch moment generated due to the thrust is fairly high. In addition, when flying at high angles of attack, a natural nose-down aerodynamic moment appears. Consequently, to be in equilibrium, the sum of these two moments has to be countered with the elevator. As it has been seen, this factor limits the configurations with fewer propellers to reach potential stall speeds. Even in those cases where the elevator is not the limiting factor, deflections are considerable, and the pilot will have reduced control if needed. Finally, as previously explained, minimizing thrust is especially important in the case of HLPs, in order to maintain higher control of the aircraft during the descent. If the thrust is too high, additional drag should be created by some means in order to slow down until the desired speed.

Following this sense, a minimization of the HLPs power will reduce both the thrust and the aircraft's power requirement. A reduction of the HLPs power allows a direct reduction of the weight through the motors and batteries resizing. At the same time, a reduction in weight leads to a lower stall speed $V_{SR}$. This reduction of weight through power minimization is, however, not considered in the loop. Instead, the reduction of weight can be seen as an opportunity to increase the payload.

A new optimization is now considered with the objective of reducing the total HLPs power. The variables of the problem remain the same as in section V, but the objective function is now the total power of the HLPs, which is intended to be minimized. The problem is written as:

$$\min_{\tilde{x}} \quad P = \min_{\tilde{x}} \sum_{i=1}^{N} f_{p,i}$$

$$\text{With:} \qquad \tilde{x} = [\alpha, \theta, V, \gamma, \delta_e]^T + \boldsymbol{D_p} + \boldsymbol{f_p}$$

Subjected to:

$$g_1 = \begin{cases} 0 = -\frac{2mg}{\rho V^2 S_w} \sin\theta + \sum_{i=1}^{N_p} C_{T,i} \cos i_p + C_L \sin\alpha - C_D \cos\alpha \\ 0 = \frac{2mg}{\rho V^2 S_w} \cos\theta - \sum_{i=1}^{N_p} C_{T,i} \sin i_p - C_L \cos\alpha - C_D \sin\alpha \\ 0 = C_{mA} - \sum_{i=1}^{N_p} C_{T,i} (\hat{z_i} \cos i_p - \hat{x_i} \sin i_p) \\ 0 = \alpha + \gamma - \theta \end{cases} \tag{23}$$

$$g_2 = \begin{cases} V_{S,orig} \geq V \\ 0 < (0.5b - R_{tip}) - (\sum_{i=1}^{N_p/2} D_p + R_{fus}) \\ 0 < 0.5 - \sum_{i=1}^{N_p/2} P_p \\ \forall D_{p,i} : n < n_{max}, \quad n_{max} = \ n: \quad M = 0.5 \end{cases} \tag{24}$$

For $N_p = 8, 10, 12, 14, 16$

**Table 13 Variables bounds**

| Variable | Bounds |
|---|---|
| Airspeed $V$ (m/s) | $20 < V < 29.42$ |
| Angle of attack $\alpha$ (°) | $-5 < \alpha < 25$ |
| Elevator $\delta_e$ (°) | $-50 < \delta_e < 40$ |
| Propeller diameter $D_{p,i}$ (m) | $0.6D_p < D_{p,i} < 2.5D_p$ |
| Propeller power fraction $f_{p,i}$ (-) | $0.01 < f_{p,i} < 0.5$ |

The upper and lower bounds for the optimization problem are presented in table 13. An additional inequality constraint is added to ($g_2$) in order to express that the stall speed $V_{SR}$ must be equal to or lower than the one achieved in the conventional version of the aircraft with the elevator limited to $\delta_e = 30°$, table 6.a. This constraint is directly implemented through modification of the upper bound for the speed $V$, (table 13). Due to the results of section V, configurations with 6 and 18 propellers are dismissed due to their inability to achieve the cited stall speed of 29.42 m/s, the first one with the elevator limited and the second one in any case.

### D. Results

The optimization results for each $N_p$ configuration are presented in figure 13, and detailed in table 14. By minimizing the power while constraining the stall speed, the resultant configurations tend to exploit all the possible means to generate the maximum lift, i.e., increasing the angle of attack until no more pitch moment can be created from the horizontal tail to counter both the thrust and the wing-body aerodynamic moment. In other words, the elevator is once again saturated or almost saturated for all the configurations.

**Table 14 Stall speed results**

| Variable | Conf ($N_p$): | 8 | 10 | 12 | 14 | 16 |
|---|---|---|---|---|---|---|
| Stall speed $V_{SR}$ (m/s) | | 29.42 | 29.42 | 29.42 | 29.42 | 29.42 |
| Angle of attack $\alpha$ (°) | | 10.8 | 10.52 | 10.1 | 9.3 | 8.7 |
| Elevator $\delta_e$ (°) | | -30 | -29.9 | -28.5 | -26.9 | -26.7 |
| Total thrust $T$ (N) | | 2555 | 2613 | 2625 | 2675 | 2671 |
| Power $P$ (kW) | | 109.31 | 112.41 | 114.35 | 118.84 | 124.51 |
| Lift Coefficient $C_L$ (-) | | 3.92 | 3.92 | 3.92 | 3.93 | 3.94 |
| Drag Coefficient $C_D$ (-) | | 0.76 | 0.78 | 0.79 | 0.79 | 0.80 |

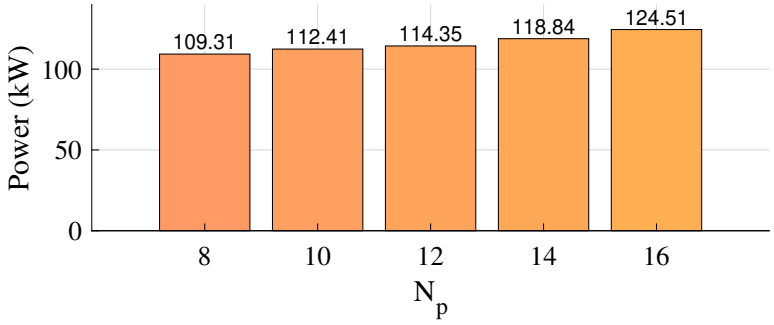


**Fig. 13 Minimum power found for each $N_p$ configuration.**

Again, for the sake of brevity, just the details of the winning configuration are shown in table 15, and the geometry

in figure 14. The resultant winning configuration possesses 8 propellers. The thrust is reduced to around 100 N with respect to the conventional version, while the power is reduced to 109.31 kW, around 8.7 % less than in the conventional version (where the thrust setting was $\delta_x$ = 0.95, with a power of P = 119.7 kW, see table 6.a), while maintaining the same stall speed $V_{SR}$ = 29.42 m/s. The resultant configuration does not differ considerably from the one from the minimization of the $V_{SR}$. Once again, the smaller propeller is placed next to the fuselage, for the same reasons as in section V. However, some additional region outside the flap is now blown. For configurations with few propellers (8, 10) this suggests the idea of positioning the first propeller further from the fuselage, making the position of this first propeller (or eventually of all propellers) a new optimization variable. Since some blowing is now outside the flap, additional power could be reduced if the first propeller is not constrained by the interaction with the downwash and the tail.

**Table 15 Winner configuration**

| **Variable** | **Value** |
|---|---|
| Number of propellers $N_p$ | 8 |
| Stall speed $V_{SR}$ (m/s) | 29.42 |
| Angle of attack $\alpha$ (°) | 10.8 |
| Diameter of the propellers $\boldsymbol{D_p^*}$ (m) | $(0.824, 0.845, 0.944, 0.509)^T$ |
| Power fraction of the propellers $\boldsymbol{f_p^*}$ (-) | $(0.111, 0.127, 0.152, 0.043)^T$ |
| Thrust $T$ (N) | 2555 |
| Power $P^*$ (kW) | 109.31 |
| Lift Coefficient $C_L$ (-) | 3.92 |
| Drag Coefficient $C_D$ (-) | 0.76 |

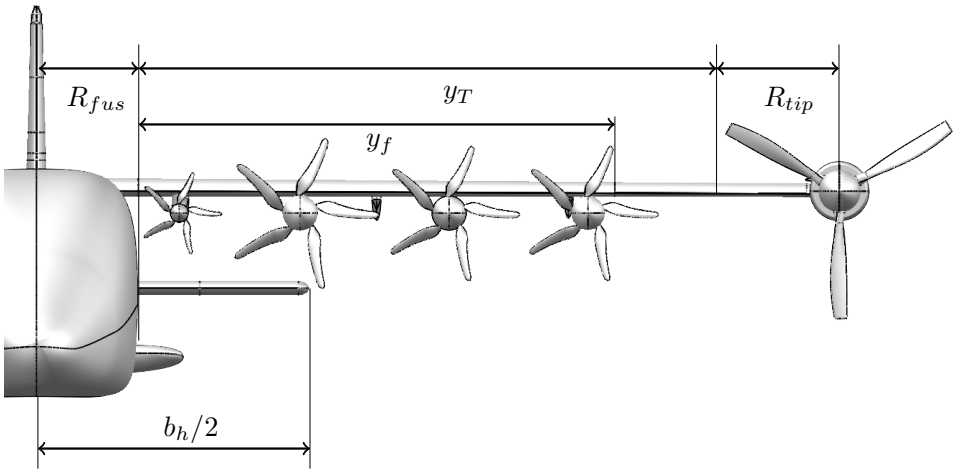


**Fig. 14 Front view of the optimized configuration for $P$ with bounded elevator**

## VI. Conclusion

The objective of this research was to study the influence of the propeller's installation parameters on the performance of a DEP aircraft. Specifically, the focus was on the enhancing lift feature provided by the aero-propulsive interaction, and the implications to achieve a reduced stall speed with a smaller wing, more optimal for cruise. The aircraft chosen to conduct this exploration was the X-57 Maxwell, an all-electric experimental aircraft that uses HLPs with this very purpose.

Through an optimal propeller installation, the stall speed $V_{SR}$ was reduced by 3.2 % (1 m/s) if a bounded elevator is considered, with a configuration of 10 propellers, or up to 6.3 % (1.8 m /s) if enough aerodynamic pitch moment can be created, with 8 propellers. In particular, in the X-57, the thrust pitch moment due to HLPs thrust is high, and considerable deflections of the elevator are required to counter it, resulting in this element being close to saturation and leaving the pilot no longer with control. The elevator is therefore found to be the limit for this stall speed in the majority of cases, instead of the power. Optimized configurations are able to achieve reduced stall speeds since they exploit more the lift augmentation provided by the flap and since propellers in front of the horizontal tail interact with it in a more favorable way, allowing to create more pitch moment. Consequently, results show that careful integration between these two elements should be taken during the preliminary design.

On the other hand, by minimizing the power, the total HLP power was reduced up to 8.7 %, by utilizing 8 propellers, while maintaining the same original stall speed $V_{SR}$ achieved by the conventional X-57 with the elevator bounded. At the same time, the thrust is also reduced, allowing more control of the approach speed during the descent maneuver. However, when installing fewer propellers, the aircraft performance is more sensitive when facing an engine failure. In addition, in optimized configurations, there is one propeller performing the majority of the propulsion and lift enhancement. Geometry is also more complicated when compared with the simplified approach of designing all the propellers equally. The reduction of power is, however, considerable, and the reduction in weight and energy consumption could be worthy, especially for an electric aircraft where endurance and range performances are a critical aspect.

The next logical step is to consider the wing's geometry and aerodynamics in the MDO loop. By increasing the wing load and reducing the stall speed of the aircraft through optimal propeller integration, the wing size is no longer over-compromised for meeting the required stall speed $V_{SR}$. A reduction of both the size of the wing and the installed HLP's power leads to a weight reduction that can be exploited for payload increase, batteries enlargement and augmented range. FAST-OAD (Future Aircraft Sizing Tool - Overall Aircraft Design) is a package for the preliminary design, analysis, and optimization of aircraft that integrates several VLM into the MDO loop and allows for this further optimization.

## Acknowledgments

The author would like to thank ISAE-Supaero, Airbus in the frame of the Chair CEDAR, and the FONISEN Federation for their investment and funding in this project.

## References

[1] Kim, H. D., Perry, A. T., and Ansell, P. J., "A Review of Distributed Electric Propulsion Concepts for Air Vehicle Technology," *2018 AIAA/IEEE Electric Aircraft Technologies Symposium*, 2018. https://doi.org/10.2514/6.2018-4998, URL https://arc.aiaa.org/doi/abs/10.2514/6.2018-4998.

[2] Patterson, M. D., and Borer, N. K., "Approach Considerations in Aircraft with High-Lift Propeller Systems," *17th AIAA Aviation Technology, Integration, and Operations Conference*, 2017. https://doi.org/10.2514/6.2017-3782, URL https://arc.aiaa.org/doi/abs/10.2514/6.2017-3782.

[3] Borer, N. K., Patterson, M. D., Viken, J. K., Moore, M. D., Bevirt, J., Stoll, A. M., and Gibson, A. R., "Design and Performance of the NASA SCEPTOR Distributed Electric Propulsion Flight Demonstrator," *16th AIAA Aviation Technology, Integration, and Operations Conference*, 2016. https://doi.org/10.2514/6.2016-3920, URL https://arc.aiaa.org/doi/abs/10.2514/6.2016-3920.

[4] Dillinger, E., Döll, C., Liaboeuf, R., Toussaint, C., Hermetz, J., Verbeke, C., and Ridel, M., "Handling qualities of ONERA's small business concept plane with Distributed Electric Propulsion," *In 31st ICAS Conference*, Belo Horizonte, Minas Gerais, Brazil, 2018.

[5] Nguyen Van, E., Alazard, D., Pastor, P., and Döll, C., "Towards an Aircraft with Reduced Lateral Static Stability Using Differential

Thrust," *2018 Aviation Technology, Integration, and Operations Conference*, 2018. https://doi.org/10.2514/6.2018-3209, URL https://arc.aiaa.org/doi/abs/10.2514/6.2018-3209.

[6] Nguyen Van, E., Alazard, D., Pastor, P., and Döll, C., "Co-design of aircraft vertical tail and control laws using distributed electric propulsion," *In IFAC Symposium on Automatic Control in Aerospace*, Cranfield, United Kingdom, Aug. 2018.

[7] Nguyen Van, E., "Lateral stability and control of an aircraft equipped with a small vertical tail by differential use of the propulsion systems. Use of co-design methods." Ph.D. thesis, ISAE-SUPAERO Institut Supérieur de l'Aéronautique et de l'Espace, Toulouse, France, Oct. 2020.

[8] Patterson, M. D., Derlaga, J. M., and Borer, N. K., "High-Lift Propeller System Configuration Selection for NASA's SCEPTOR Distributed Electric Propulsion Flight Demonstrator," *16th AIAA Aviation Technology, Integration, and Operations Conference*, 2016. https://doi.org/10.2514/6.2016-3922, URL https://arc.aiaa.org/doi/abs/10.2514/6.2016-3922.

[9] Fei, X., German, B., and Patterson, M. D., "Exploring the Effects of Installation Geometry in High-Lift Propeller Systems," *2018 AIAA Aerospace Sciences Meeting*, 2018. https://doi.org/10.2514/6.2018-0277, URL https://arc.aiaa.org/doi/abs/10.2514/6.2018-0277.

[10] Gentry, G., Takallu, M., and Applin, Z., "Aerodynamic Characteristics of a Propeller-Powered High-Lift Semispan Wing," *National Aeronautics and Space Administration Langley Research Center*, 1994.

[11] Veldhuis., L., "Propeller Wing Aerodynamic Interference." Ph.D. thesis, Delft University of Technology, The Netherlands, 2005.

[12] Chauhan, S. S., and Martins, J. R. R. A., "RANS-based aerodynamic shape optimization of a wing considering propeller-wing interaction," *AIAA Scitech 2020 Forum*, 2020. https://doi.org/10.2514/6.2020-1764, URL https://arc.aiaa.org/doi/abs/10.2514/6.2020-1764.

[13] Clarke, M. A., Erhard, R. M., Smart, J. T., and Alonso, J., "Aerodynamic Optimization of Wing-Mounted Propeller Configurations for Distributed Electric Propulsion Architectures," *AIAA AVIATION 2021 FORUM*, 2021. https://doi.org/10.2514/6.2021-2471, URL https://arc.aiaa.org/doi/abs/10.2514/6.2021-2471.

[14] Alba, C., Elham, A., German, B. J., and Veldhuis, L. L., "A surrogate-based multi-disciplinary design optimization framework modeling wing–propeller interaction," *Aerospace Science and Technology*, Vol. 78, 2018, pp. 721–733. https://doi.org/https://doi.org/10.1016/j.ast.2018.05.002, URL https://www.sciencedirect.com/science/article/pii/S1270963818303481.

[15] Bouquet, T., and Vos, R., "Modeling the Propeller Slipstream Effect on Lift and Pitching Moment," *55th AIAA Aerospace Sciences Meeting*, 2017. https://doi.org/10.2514/6.2017-0236, URL https://arc.aiaa.org/doi/abs/10.2514/6.2017-0236.

[16] Bohari, B., Bronz, M., Bernard, E., and Borlon, Q., "Conceptual Design of Distributed Propellers Aircraft: Linear Aerodynamic Model Verification of Propeller-Wing Interaction in High-Lifting Configuration," *7 TH EUROPEAN CONFERENCE FOR AERONAUTICS AND AEROSPACE SCIENCES (EUCASS)*, 2017. https://doi.org/10.2514/6.2018-1742.

[17] McDonald, R. A., and Gloudemans, J. R., "Open Vehicle Sketch Pad: An Open Source Parametric Geometry and Analysis Tool for Conceptual Aircraft Design," *AIAA SCITECH 2022 Forum*, January, 2022. https://doi.org/10.2514/6.2022-0004, URL https://arc.aiaa.org/doi/abs/10.2514/6.2022-0004.

[18] Etkyns, B., *Dynamics of flight. Stability and Control*, 3rd ed., John Wiley & Sons, USA, 1996.

[19] Done, G., "Dynamics of Flight: the Equations. J.-L. Boiffier. John Wiley and Sons, Baffins Lane, Chichester, West Sussex P019 1UD, UK1998. 353 pp. Illustrated. £34.95." *The Aeronautical Journal*, Vol. 103, No. 1026, 1999, p. 362–362. https://doi.org/10.1017/S0001924000064563.

[20] McCormick, B., *Aerodynamics of v/stol flight.*, Dover Publications, 1999.

[21] Drela, M., "XFOIL: An Analysis and Design System for Low Reynolds Number Airfoils," *Low Reynolds Number Aerodynamics*, edited by T. J. Mueller, Springer Berlin Heidelberg, Berlin, Heidelberg, 1989, pp. 1–12.

[22] Jameson, A., "Analysis of wing slipstream flow interaction," *NASA Contractor Reports*, 1970.

[23] Obert., E., "The effect of propeller slipstream on the static longitudinal stability and control of multi-engined propeller aircraft." *Delf University of Technology*, 1994.

[24] Planas, D., Pastor, P., and Döll, C., "Handling Qualities of a distributed propulsion electric aircraft," *In ICAS International Council of Aeronautical Sciences*, Stockholm, Sweden, 2022.

[25] Viken, J. K., Viken, S., Deere, K. A., and Carter, M., "Design of the Cruise and Flap Airfoil for the X-57 Maxwell Distributed Electric Propulsion Aircraft," *35th AIAA Applied Aerodynamics Conference*, 2017. https://doi.org/10.2514/6.2017-3922, URL https://arc.aiaa.org/doi/abs/10.2514/6.2017-3922.

[26] Litherland, B. L., Borer, N. K., and Zawodny, N. S., "X-57 Maxwell High-Lift Propeller Testing and Model Development," *AIAA AVIATION 2021 FORUM*, 2021. https://doi.org/10.2514/6.2021-3193, URL https://arc.aiaa.org/doi/abs/10.2514/6.2021-3193.

[27] Yoo, S., and Duensing, J., "Computational Analysis of the External Aerodynamics of the Unpowered X-57 Mod-III Aircraft," *AIAA Aviation 2019 Forum*, 2019. https://doi.org/10.2514/6.2019-3698, URL https://arc.aiaa.org/doi/abs/10.2514/6.2019-3698.

[28] Duensing, J., Housman, J., Maldonado, D., Jensen, J., Kiris, C., and Yoo, S., "Computational Simulations of Electric Propulsion Aircraft: the X-57 Maxwell," , 2019. URL https://www.nas.nasa.gov/pubs/ams/2019/06-13-19.html.

[29] Kraft, D., "A software package for sequential quadratic programming," *Tech. Rep. DFVLR-FB 88-28, DLR German Aerospace Center — Institute for Flight Mechanics*, Koln, Germany, 1988.

[30] Vos, R., and Bouquet, T., "Modeling the Propeller Slipstream Effect on Lift and Pitching Moment," *In 55th AIAA Aerospace Sciences Meeting*, 2017.